Use of an Underlayer for Large Area Crystallization of Rubrene Thin Films

Michael A. Fusella[1], Siyu Yang[1], Kevin Abbasi[2], Hyun Ho Choi[3], Zhuozhi Yao[1], Vitaly Podzorov[3], Amir Avishai[2], and Barry P. Rand[1,4*]

[1]Department of Electrical Engineering, Princeton University, Princeton, NJ 08544 USA.

[2]Swagelok Center for Surface Analysis of Materials, Case Western Reserve University, Cleveland, OH 44106 USA.

[3]Department of Physics and Astronomy, Rutgers University, Piscataway, NJ USA.

[4]Andlinger Center for Energy and the Environment, Princeton University, Princeton, NJ 08544 USA.

*Correspondence to: brand@princeton.edu

Abstract

In this work we have discovered a very efficient method of crystallization of thermally evaporated rubrene resulting in ultra-thin, large-area, fully connected and highly crystalline thin films of this organic semiconductor with a grain size of up to 500 μm and charge carrier mobility of up to 3.5 $cm^2V^{-1}s^{-1}$. We have found that it is critical to use a 5 nm-thick organic underlayer, on which a thin film of amorphous rubrene is evaporated and then annealed, to dramatically influence the ability of rubrene to crystallize. The underlayer property that controls this influence is the glass transition temperature. By experimenting with different underlayers with glass transition temperatures varying over 120 ˚C, we have identified the molecules leading to the best crystallinity of rubrene films and explained why values both above and below the optimum result in poor crystallinity. We discuss the formation of different crystalline morphologies of rubrene produced by this method and show that field-effect transistors made with films of a single-domain platelet morphology, achieved through the aid of the optimal underlayer, outperform their spherulite counterparts with a nearly four times higher charge carrier mobility. This

large-area crystallization technique overcomes the fabrication bottleneck of high-mobility rubrene thin film transistors and other related devices, and, given its scalability and patternability, may lead to practical technologies compatible with large-area flexible electronics.

Table of Contents Figure

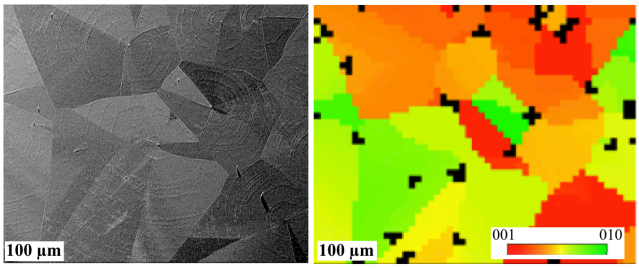

Introduction

Organic electronics hold the promise of low-cost, low-temperature, and large-area fabrication that is suitable for flexible substrates.[1] To achieve these practical aspirations, however, successful control over the structural order of organic thin films, which are typically largely disordered, is essential. While organic single crystals have demonstrated impressive electrical performance with diffusion lengths in rubrene up to 8 μm (ref. 2) and consistently high FET mobilities,[3] there is limited scope to grow single crystals on a substrate, whereas thin films possess the potential for incorporation into large-scale fabrication methods. Toward this end, researchers have sought to enhance the crystallinity of thin films by growing on self-assembled monolayers[4] or inert substrates,[5] or by using techniques such as organic vapor phase deposition,[4] organic epitaxy,[6] structural templating,[7] and substrate-induced phases.[8]

Rubrene, an archetypal small molecule, is a benchmark material in organic electronics, having demonstrated FET mobilities up to 20 $cm^2V^{-1}s^{-1}$ and band-like charge transport in single crystals.[9,10] Rubrene is known to have at least three distinct crystal phases, though typically its thin films are amorphous. To overcome this, solution processed rubrene films have introduced polymer binders,[11] or incorporated a glass-inducing diluent[12] to control crystallinity. Additionally, a post-processing technique has been investigated[13-15] to transform thermally evaporated amorphous rubrene thin films via an abrupt heating mechanism into crystalline films of the orthorhombic polymorph with typical grain sizes on the order of 10s of microns. Though successful, this technique is highly sensitive to the annealing conditions and film thickness, and must contend with growth of the lower-electrically-performing and therefore less desirable triclinic

polymorph at temperatures just below orthorhombic nucleation.[13,15] Here, we show that the inclusion of a thin (5 nm) organic underlayer between the substrate and rubrene film dramatically influences the crystallization process and makes it possible to yield complete, crystalline thin films of the orthorhombic polymorph with single-crystal domains on the order of 100s of microns. We investigate the effects of including such an underlayer to aid in the crystallization of rubrene thin films and find that the underlayer's glass transition temperature (T_g) is the primary factor in determining the qualities of the crystalline film. Finally, we discuss the formation of the single-crystal domains in the resulting film.

Results and Discussion

We investigated six different molecules as underlayers, with their molecular structures shown in Fig. 1a: tris(8-hydroxyquinolinato)aluminum (Alq_3), N,N'-bis(naphthalen-1-yl)-N,N'-bis(phenyl)benzidine (NPB); tris[4-(5-phenylthiophen-2-yl)phenyl]amine (TPTPA); 4,4',4"-tris[phenyl(m-tolyl)amino]triphenylamine (m-MTDATA); N,N,N',N'-tetrakis(4-methoxy-phenyl)benzidine (MeO-TPD); and N,N′-bis(3-methylphenyl)-N,N′-diphenylbenzidine (TPD). These molecules were chosen because their T_g span a wide (~120 ˚C) temperature range, specific values of which are reported in Table 1. Additionally, they are all pi-conjugated semiconductors, produce amorphous thin films via thermal evaporation, and do not crystallize over the relevant rubrene crystallization temperature range (130-170 ˚C). To fabricate the samples, the underlayer is deposited onto a glass/indium tin oxide (ITO) substrate followed by rubrene (Fig. 1b). Though underlayer thicknesses from 5 – 30 nm were investigated, 5 nm films always yielded the highest quality rubrene crystals so only results for 5 nm underlayers

are reported here. The rubrene film thickness was also optimized from 10 – 40 nm for each underlayer and annealing temperature.

As a control, we anneal a 20 nm thick rubrene film at 140 ˚C directly on glass/ITO (i.e. no underlayer) and find that the resulting film predominantly consists of needle-shaped crystallites with small pockets of uniformly colored grains, as seen in the polarized optical microscope (POM) image in Fig. 2a. These needle-shaped crystallites have been investigated previously[13,15] and were found to exhibit the triclinic rubrene polymorph, whereas the uniformly colored grains comprise the orthorhombic polymorph. The triclinic phase is electrically inferior to its orthorhombic counterpart, exhibiting low mobility,[16] and produces rough films unsuitable for device applications. In contrast, large (100s of microns), single-domain orthorhombic crystallites, which we refer to as "platelets," are particularly desirable. In an effort to more precisely control the phase of the crystalline film, we investigate how the underlayer influences the crystallization of the rubrene film. In particular, we have selected underlayers with T_g values both *above* and *below* the typical rubrene thin film crystallization range to see the effect of a rigid (high T_g) or mobile (low T_g) underlayer on rubrene crystallization.

However, because T_g of an organic thin film is a function of its thickness, we utilize ellipsometry measurements[17] (Fig. S1a) to determine T_g for thicknesses that approach that of the underlayer. We find that, for the underlayers investigated here, T_g decreases with decreasing film thickness (Fig. S1b). However, measurements using this technique become less reliable as film thickness decreases and we are unable to confidently measure T_g for films thinner than 20 nm. Nonetheless, we find that the ordering of the underlayer T_g is the same for every film thickness measured; thus we only

report the measured T_g for a 70 nm thick film in Table 1 since these films yielded the most accurate values. We also note that measurements for Alq_3 were unsuccessful as the films dewetted from the substrate surface before a T_g value could be measured; thus we will refer only to the value reported for bulk Alq_3.

To investigate the effect on rubrene thin film crystallization, we introduce an underlayer and keep the rubrene thickness and the annealing temperature the same as our control (20 nm and 140 ˚C, respectively). The molecule with the highest T_g, Alq_3, has a bulk T_g above the annealing temperature, which means that the underlayer will remain rigid during annealing, similar to the glass/ITO control. Indeed, the resulting crystalline rubrene film (Fig. 2b) is very similar to the control in that only the triclinic polymorph is present. Switching to NPB brings the underlayer T_g below the annealing temperature and in Fig. 2c we see that though there are some uniformly colored grains, the majority of grains exhibit intra-grain color gradients. This indicates the presence of misoriented crystal regions resulting from polycrystalline branching typical of spherulite growth.[18] Due to a large increase in the number of grain boundaries, spherulites are less desirable than uniformly colored, and hence single-domain, platelets. Lowering the underlayer T_g further, we investigate the use of TPTPA and m-MTDATA, which have very similar T_g values. Indeed, the resulting crystalline rubrene films (Figs. 2d and e, respectively) closely resemble each other as both films display large, uniformly colored grains. This seems to suggest that low T_g underlayers are more capable than their high T_g counterparts in achieving platelet growth. However, as we continue to lower the T_g of the underlayer through the use of MeO-TPD (Fig. 2f), and even further with TPD (Fig. 2g), we find that the rubrene crystallites trend back toward spherulites as the grains exhibit a “splitting”

phenomenon that results in an increase in the number of "rays" per crystallite. Some crystallites even display the radial color gradient characteristic of spherulites.

It is important to consider that the rubrene film thickness and annealing conditions need to be optimized for each underlayer and it is possible that unsuccessful crystallizations (i.e. not resulting in platelet formation) in Fig. 2 may yet become successful once optimized. The results of Fig. 3, however, show that even under optimal conditions the trends uncovered in Fig. 2 are upheld. The Alq_3 underlayer is able to achieve orthorhombic rubrene crystals with a thicker (40 nm) rubrene film but only at a higher temperature (160 ˚C), which ultimately results in a spherulite film (Fig. 3a). The optimal conditions for the NPB underlayer occur when the rubrene thickness increases to 30 nm and the annealing temperature increases to 150 ˚C at which point the film (Fig. 3b) exhibits many uniformly colored grains that are, however, still interspersed with grains displaying significant splitting or large numbers of rays. The optimal conditions for the remaining underlayers (Figs. 3c-f) are the same as those from Fig. 2.

We now exclude other effects that may influence the crystallization behavior. To make certain that the underlayer surface energy does not play a significant role in these findings, we measure the surface energy of a 5 nm film of each molecule via contact angle analysis. The results, shown in Table 1, confirm that the surface energy is largely the same or within error across all molecules investigated here and therefore is not the dominant effect behind these results. We also note that the smoothness of the substrate does not (to within the experimental conditions) influence the crystallization behavior. In Fig. 2a,b,c,e,f, the left half of the image is grown on ITO whereas the right half is grown on glass. As can be seen in the images, the resulting crystalline films are essentially

identical. Additionally, we can exclude the effects of intermixing or miscibility that may be present between the underlayer and rubrene films. In Fig. S3 we show that the effect of the underlayer diminishes with increasing rubrene thickness, and that crystallization becomes unsuccessful as the underlayer gets too thick. Since the degree of intermixing, if present, would not depend on the film thicknesses (i.e. no significant roughening is expected for amorphous films), we can exclude intermixing as a dominant factor to explain the large differences in crystallization behavior seen with changing film thickness. Further, since all underlayers investigated in this work are amorphous and chemically similar, we can assume approximately the same level of intermixing/miscibility for each sample, and thus these effects would be unable to explain the varying results on rubrene crystallization between the different underlayers.

Finally, the fact that our systematic modulation of T_g has resulted in the identification of two successful underlayers with similar T_g, bounded by underlayers that are unfavorable for having T_g "too high" and "too low" makes a compelling argument that the glass transition temperature is the primary parameter that determines these crystallization differences.

To understand these results we provide the following hypothesis. A rubrene molecule in a supersaturated, amorphous film must rotate in order to align itself with the crystallization growth front, which will necessarily require the movement of surrounding molecules. It is reasonable to expect that the in-plane shear force will be much higher than in the out-of-plane z-direction since, to a given rubrene molecule in the film, the in-plane lattice is quasi-infinite whereas the out-of-plane lattice is only approximately 10 – 30 molecules thick; thus the crystallization process should be dominated by molecular

rotation dynamics. Having an underlayer below the rubrene film that is above its glass transition temperature during annealing will therefore assist (or, at the very least, not hinder) the rubrene molecules to rotate into alignment with the parent crystal, thus enabling formation of large, platelet grains. In the language of potential energy, a mobile underlayer enables the rubrene molecules to explore various energy positions to find the lowest one and attach to the growing crystal.

With a rigid substrate such as glass/ITO or an underlayer whose T_g is high or even *above* the annealing temperature, the molecular rotation of rubrene will be slowed down. This is because the rigid underlayer impedes the ability of the molecules to rotate, as it no longer provides the essential mobility in the z-direction and thus requires a rubrene molecule to push others away to achieve rotation. As was the case with Alq_3, orthorhombic domains could only be achieved at higher temperatures, which not only increases the rate of molecular rotation but also the rate of crystallization. The resulting spherulite growth (Fig. 3a) is evidence that the faster crystallization rate dominates. In this case, the rubrene molecules are unable to probe a sufficient number of orientations before they must join the crystal and thus polycrystalline branching occurs. It is also notable that, for a given annealing temperature (i.e. 140 ˚C, as in Fig. 2), either spherulites or platelets are able to form depending on the underlayer (i.e. NPB vs. TPTPA or m-MTDATA). To explain this observation, we propose that the more rigid underlayer (NPB) hinders molecular rotation to the point where the rubrene molecules are unable to reach optimal alignment by the time they must join the crystal, which thus results in branching.

While it seems logical that an underlayer with T_g above the annealing temperature – or one that is otherwise too rigid – should produce films similar to those annealed on glass or ITO, it is perhaps counterintuitive that there should be a lower limit to the T_g of a successful underlayer as well. We can understand this by again considering the role of the underlayer in assisting rubrene molecules to rotate. An underlayer annealed at a temperature far above its T_g will be extremely mobile, which turns out to be detrimental to a rubrene molecule trying to align itself with the growing crystal. As the neighboring crystal is agitated more vigorously as a result of the mobile underlayer, it becomes increasingly difficult for a rubrene molecule to find the optimum position for alignment. A very fluid underlayer may even change the energy minimum of the crystal or may make the energy minimum disappear frequently, thus making it difficult for a rubrene molecule to find a definite energy minimum as it adds itself to the crystal. The crystal splitting seen in Figs. 3e and f might also be explained by a vigorously mobile underlayer that is able to knock rubrene molecules out of alignment even after they have joined the crystal, thereby causing misorientations. We note that molecular diffusion/translation also plays a role in the crystallization of rubrene; however, we assert that the enhancement of molecular rotation enabled by the soft underlayer is what dominates the ability to form large platelet crystals. This has been discussed by Gránásy, et al.[18] who argue that if the ratio of molecular rotational to translational diffusion coefficients is large then crystals with low degrees of misorientation will form (i.e. platelets). In contrast, if the ratio is small (as with a rigid underlayer), it favors polycrystalline branching (i.e. spherulites).

It should be noted that these conclusions, i.e. that an underlayer whose T_g is *below* the annealing temperature works better than one whose T_g is *above* the annealing

temperature, are in contrast to works previously reported for crystalline films grown using this annealing method on polystyrene[19,20] that claim better crystallization when the underlayer T_g is *above* the annealing temperature. However, those works did not fully investigate the effect of T_g on crystallization behavior and did not, for instance, consider subtleties such as the lowering of T_g with decreasing film thickness.

A striking feature of Fig. 3 is that, under optimal annealing conditions for a given underlayer, the resulting rubrene crystallites display a wide variation in form, from platelets with large, single-colored rays to spherulites. For TPTPA and m-MTDATA underlayers, the accessible transition from platelet to spherulite provides a deeper understanding of the formation of the rubrene crystallites. Shown in Fig. 4 for a TPTPA underlayer, we define n as the number of single-colored rays in a given domain. In a complete film at a given temperature there will be a distribution of n-values but we find that increasing the annealing temperature increases the average n-value, from small values (Fig. 4a, annealed at 140 ˚C) to larger values (Figs. 4b-d) and enables a transition from platelets to spherulites, whereby the rays are so small ($n \approx \infty$) that a radial color gradient, indicating molecular misorientation due to polycrystalline branching, is seen via POM (Fig. 4e, annealed at 170 ˚C). This transition can be explained by the competition between molecular rotational correlation time, which describes the rotational motion of a sphere in a hydrodynamic continuum of a certain viscosity and temperature,[21] and the increasing nucleation and crystal growth rates as the annealing temperature rises. Indeed, with an m-MTDATA or TPTPA underlayer it takes up to 7 min to form a complete platelet film annealing at 140 ˚C, whereas it takes 1 min or less to form a complete spherulite film at 170 ˚C. The unique aspect of the range of small n-values is not only that

it produces rubrene domains with crystallite rays of different in-plane rotations, but also that these rays begin at the nucleation point and maintain their uniform color throughout the entire growth process. We hypothesize that at low temperatures the molecules have enough time to rotationally align themselves to form a single-crystal nucleus, whereas at higher temperatures nucleation occurs before perfect rotational alignment can occur, thereby creating an imperfection in the crystal nucleus that subsequently causes growth of distinct rays. However, the crystal growth front propagation itself is still slow enough for additional molecules to rotate into alignment before attaching to the growing parent crystal, thereby maintaining the uniform coloring of the rays for the remainder of the crystal growth. Additional images investigating the effects of annealing temperature, and rubrene and underlayer film thickness for various underlayers are shown in Figs. S2 and S3, respectively.

The fact that each ray possesses a distinct color when imaged via POM suggests that each exhibits a different in-plane rotation of the rubrene molecules. We are able to confirm this in-plane rotation and the assertion that each uniquely colored grain is a distinct crystal domain via electron backscatter diffraction (EBSD). Figure 5a shows a forward scattered scanning electron microscope (SEM) image of the crystalline rubrene thin film and an EBSD orientation map of the same area is presented in Figs. 5b and c. Each uniquely shaded area in the EBSD orientation map in Fig. 5b denotes a different grain and in-plane molecular orientation and demonstrates excellent agreement with the SEM image. The uniform coloring of the map in Fig. 5c shows that all grains are oriented with the a-axis out-of-plane. To the best of our knowledge, these orientation maps are the first of their kind for organic thin films. From the texture analysis displayed in the pole

figures in Fig. S4, we can assert that rotation in the (111) and (110) planes (i.e. in-plane) is predominantly random.

Finally, we fabricate top-gate rubrene thin film transistors (TFTs) on films with platelet and spherulite morphologies, each with a 5 nm underlayer of TPTPA, and compare the performance of these TFTs (Fig. 6). We find that transistors based on the platelet morphology exhibit a linear field-effect mobility of μ = 3-4 $cm^2V^{-1}s^{-1}$, a nearly four-fold improvement over μ = 0.8-1.2 $cm^2V^{-1}s^{-1}$ observed in TFTs utilizing the spherulite morphology. This correlation is reproducible, with additional TFTs yielding consistent mobilities (Fig. S5). We attribute this enhancement of carrier mobility in the platelet morphology to the absence of intra-domain (low-angle) grain boundaries common for the spherulite films. The mobilities presented here for rubrene thin films with the platelet morphology are nearly four times higher than μ previously reported for crystalline rubrene thin films[13,19] and are only a factor of ~ 2-3 lower than typical μ in discrete high-purity rubrene single-crystal OFETs with analogous polymeric gate insulators.[9] The relatively low on/off ratio of 10^1 - 10^2 (Fig. S6b and c) is likely due to the bottom ITO layer weakly shunting the channel. Still, the greatly enhanced mobility of the platelet rubrene thin films coupled with the ease of the underlayer processing method underscores the practical importance of this work.

Conclusion

We have demonstrated how the use of an organic underlayer can greatly impact the crystallization of rubrene thin films formed via post-deposition annealing. The most successful underlayers, m-MTDATA and TPTPA, aid in the formation of rubrene platelet crystals, which are highly desirable due to their large size and low ratio of grain

boundaries to domain size, which we have shown improves thin film transistor performance compared to the spherulite morphology. Indeed, these platelets exhibit single-domain qualities over 100s of microns, as mapped via EBSD, that are highly oriented out-of-plane but randomly oriented in-plane. We have found that the precise level of control over the formation of the crystalline rubrene film offered by a successful underlayer is due to its glass transition temperature. An underlayer with a T_g too high inhibits molecular rotation thereby making it more difficult to crystallize, which often results in polycrystalline branching (i.e. spherulites), while an underlayer with a T_g too low frustrates the ability of the molecules to successfully align with the parent crystal and causes crystallite splitting. The optimum T_g assists molecular rotation, thereby allowing the rubrene molecule to achieve proper alignment to join the growing crystal. We believe that the incorporation of an underlayer to aid in the crystallization of disordered thin films can be applied to organic systems other than rubrene, provided that the material to be crystallized is amorphous as-deposited (providing a low nucleation density) and can crystallize. The ability of this method to improve the crystallization of an archetypal molecule such as rubrene while preserving the practicality of thin films underscores the usefulness of this technique to incorporate into the next generation of organic electronic devices.

Methods

All samples were fabricated using thermal evaporation with a base pressure ~10^{-7} Torr. Substrates for crystallization and surface energy measurements were pre-patterned ITO on glass, whereas silicon with native oxide was used for ellipsometry samples. All

materials were purchased from commercial vendors: Rubrene (Nichem), TPTPA (Lumtec), MeO-TPD (Sigma-Aldrich), Alq_3 (Nichem), TPD (Sigma-Aldrich), m-MTDATA (Sigma-Aldrich), NPB (Nichem). Rubrene and TPTPA were purified by thermal gradient sublimation prior to use; all other materials were used as received. All substrates were cleaned by successive sonication in deionized water, acetone, and isopropanol before receiving an oxygen plasma treatment. Crystallization samples were annealed in a nitrogen glovebox by placing them directly onto a pre-heated hotplate. Subsequent polarized optical microscope images were taken with an Olympus BX60F5.

Ellipsometry measurements of the glass transition temperature were obtained using a J. A. Woollam M-2000 variable angle spectroscopic ellipsometer equipped with a heating stage and the CompleteEASE software. The measurement utilized a wavelength of 755 nm at an angle of 75˚ from the normal, and a heating rate of 6 ˚C/min. The glass transition is set as the intersection point between linear fits to the glassy and rubbery slopes (see Fig. S1a).

Surface energy was measured via contact angle. Each measurement was taken on a 5 nm film deposited on ITO. Contact angles from a series of both water and glycerol drops were used in conjunction with the Owens-Wendt-Rabel-Kaelble (OWRK) method[27] to calculate surface energy.

An FEI Nova Nanolab 200 FEG-SEM scanning electron microscope was used to image the microstructure of 100 nm thick crystalline rubrene films[28] at an acceleration voltage of 10 kV and a current of 3.7 nA. The microscope was equipped with an Oxford Nordlys Nano EBSD detector with forescattered detector diodes to incorporate forward scattered imaging capability. Surface roughness contrast was combined with orientation

contrast in a single image. EBSD was acquired by analysis of individual patterns obtained from rastering the beam on a grid in the area shown in the SEM image. The registered patterns were then matched with the reference rubrene crystal file[29] to determine the orientation of the crystal domains in terms of three Euler angles. The Euler angles were then used to calculate the pole figures using the OXFORD HKL Channel 5 software.

Top-gated thin film transistors were fabricated on glass/ITO substrates. The vertical structure of the device is presented in Fig. S6a. An insulating 100 nm-thick aluminum oxide was grown on top of the ITO via atomic layer deposition to prevent a residual current through conducting ITO. Purified rubrene and unpurified TPTPA were deposited via thermal evaporation. Crystallization was achieved by annealing the samples in a nitrogen glovebox by placing them directly onto a pre-heated hotplate. The platelet devices were annealed at 140 ˚C for 6 minutes and the spherulite devices were annealed at 165 ˚C for 45 - 60 seconds. An 80 nm thick adlayer of rubrene was deposited on top of the crystalline template at 1 Å/s and room temperature, which has been shown to propagate the crystallinity.[28] Graphite source-drain contacts were painted onto the rubrene film using a water-soluble graphite ink and then gold wires were attached to the graphite contacts as contact leads. The device was subsequently capped by layers of cytop and parylene-*N* gate dielectrics with thicknesses of 100 nm and 1.61 μm, respectively. The total capacitance is 1.354 nF cm^{-2}. Finally, a patterned ITO gate was sputtered with a thickness of 50 nm. Keithley Source-Meter K2400 and Electrometer K6512 were used for FET measurements. All measurements were performed in a dry environment.

Supporting Information Available: Figures S1-S6. This material is available free of charge *via* the Internet at http://pubs.acs.org.

Acknowledgements

The authors thank Prof. Sigurd Wagner for helpful discussions. We acknowledge support for this work from the U.S. Department of Energy, Office of Basic Energy Sciences, Division of Materials Sciences and Engineering under Award #DE-SC0012458.

References

1. Forrest, S. R. The Path to Ubiquitous and Low-Cost Organic Electronic Appliances on Plastic. *Nature* **2004**, *428* (6986), 911–918.
2. Najafov, H.; Lee, B.; Zhou, Q.; Feldman, L. C.; Podzorov, V. Observation of Long-Range Exciton Diffusion in Highly Ordered Organic Semiconductors. *Nat. Mater.* **2010**, *9* (11), 938–943.
3. Minder, N. A.; Ono, S.; Chen, Z.; Facchetti, A.; Morpurgo, A. F. Band-Like Electron Transport in Organic Transistors and Implication of the Molecular Structure for Performance Optimization. *Adv. Mater.* **2011**, *24* (4), 503–508.
4. Shtein, M.; Mapel, J.; Benziger, J. B.; Forrest, S. R. Effects of Film Morphology and Gate Dielectric Surface Preparation on the Electrical Characteristics of Organic-Vapor-Phase-Deposited Pentacene Thin-Film Transistors. *Appl. Phys. Lett.* **2002**, *81* (2), 268-270.
5. Verlaak, S.; Steudel, S.; Heremans, P.; Janssen, D.; Deleuze, M. S. Nucleation of Organic Semiconductors on Inert Substrates. *Phys. Rev. B* **2003**, *68* (19), 195409.
6. Schreiber, F. Organic Molecular Beam Deposition: Growth Studies Beyond the First Monolayer. *Phys. Stat. Sol. (a)* **2004**, *201* (6), 1037–1054.
7. Hinderhofer, A.; Gerlach, A.; Broch, K.; Hosokai, T.; Yonezawa, K.; Kato, K.; Kera, S.; Ueno, N.; Schreiber, F. Geometric and Electronic Structure of Templated C_{60} on Diindenoperylene Thin Films. *J. Phys. Chem. C* **2013**, *117* (2), 1053–1058.
8. Jones, A. O. F.; Chattopadhyay, B.; Geerts, Y. H.; Resel, R. Substrate‐Induced and Thin‐Film Phases: Polymorphism of Organic Materials on Surfaces. *Adv. Funct. Mater.* **2016**, *26* (14), 2233–2255.

9. Okada, Y.; Sakai, K.; Uemura, T.; Nakazawa, Y.; Takeya, J. Charge Transport and Hall Effect in Rubrene Single-Crystal Transistors Under High Pressure. *Phys. Rev. B* **2011**, *84* (24), 245308.
10. Podzorov, V.; Menard, E.; Borissov, A.; Kiryukhin, V.; Rogers, J. A.; Gershenson, M. E. Intrinsic Charge Transport on the Surface of Organic Semiconductors. *Phys. Rev. Lett.* **2004**, *93* (8), 086602.
11. Jo, P. S.; Duong, D. T.; Park, J.; Sinclair, R.; Salleo, A. Control of Rubrene Polymorphs via Polymer Binders: Applications in Organic Field-Effect Transistors. *Chem. Mater.* **2015**, *27* (11), 3979–3987.
12. Stingelin-Stutzmann, N.; Smits, E.; Wondergem, H.; Tanase, C.; Blom, P.; Smith, P.; de Leeuw, D. Organic Thin-Film Electronics From Vitreous Solution-Processed Rubrene Hypereutectics. *Nat. Mater.* **2005**, *4* (8), 601–606.
13. Lee, H. M.; Moon, H.; Kim, H.-S.; Kim, Y. N.; Choi, S.-M.; Yoo, S.; Cho, S. O. Abrupt Heating-Induced High-Quality Crystalline Rubrene Thin Films for Organic Thin-Film Transistors. *Org. Electron.* **2011**, *12* (8), 1446–1453.
14. Verreet, B.; Heremans, P.; Stesmans, A.; Rand, B. P. Microcrystalline Organic Thin-Film Solar Cells. *Adv. Mater.* **2013**, *25* (38), 5504–5507.
15. Fielitz, T. R.; Holmes, R. J. Crystal Morphology and Growth in Annealed Rubrene Thin Films. *Cryst. Growth Des.* **2016**, *16* (8), 4720-4726.
16. Luo, L.; Liu, G.; Huang, L.; Cao, X.; Liu, M.; Fu, H.; Yao, J. Solution-Based Patterned Growth of Rubrene Nanocrystals for Organic Field Effect Transistors. *Appl. Phys. Lett.* **2009**, *95* (26), 263312–263314.

17. Kim, J. H.; Jang, J.; Zin, W.-C. Thickness Dependence of the Glass Transition Temperature in Thin Polymer Films. *Langmuir* **2001**, *17* (9), 2703–2710.

18. Gránásy, L.; Pusztai, T.; Tegze, G.; Warren, J. A.; Douglas, J. F. Growth and Form of Spherulites. *Phys. Rev. E* **2005**, *72* (1), 011605.

19. Kim, J. J.; Lee, H. M.; Park, J. W.; Cho, S. O. Patterning of Rubrene Thin-Film Transistors Based on Electron Irradiation of a Polystyrene Dielectric Layer. *J. Mater. Chem. C* **2015**, *3* (11), 2650–2655.

20. Jang, M.; Baek, K. Y.; Yang, H. Optimization of Temperature-Mediated Organic Semiconducting Crystals on Soft Polymer-Treated Gate Dielectrics. *J. Phys. Chem. C* **2013**, *117* (48), 25290–25297.

21. Blackburn, F. R.; Wang, C. Y.; Ediger, M. D. Translational and Rotational Motion of Probes in Supercooled 1,3,5-Tris(Naphthyl)Benzene. *J. Phys. Chem.* **1996**, *100* (46), 18249–18257.

22. Cölle, M.; Gmeiner, J.; Milius, W.; Hillebrecht, H.; Brütting, W. Preparation and Characterization of Blue‐Luminescent Tris(8‐Hydroxyquinoline)‐Aluminum (Alq3). *Adv. Funct. Mater.* **2003**, *13* (2), 108–112.

23. Yin, S.; Shuai, Z.; Wang, Y. A Quantitative Structure−Property Relationship Study of the Glass Transition Temperature of OLED Materials. *J. Chem. Inf. Comput. Sci.* **2003**, *43* (3), 970–977.

24. Kageyama, H.; Ohishi, H.; Tanaka, M.; Ohmori, Y.; Shirota, Y. High-Performance Organic Photovoltaic Devices Using a New Amorphous Molecular Material with High Hole Drift Mobility, Tris[4-(5-Phenylthiophen-2-Yl)Phenyl]Amine. *Adv. Funct. Mater.* **2009**, *19* (24), 3948–3955.

25. Murawski, C.; Fuchs, C.; Hofmann, S.; Leo, K.; Gather, M. C. Alternative P-Doped Hole Transport Material for Low Operating Voltage and High Efficiency Organic Light-Emitting Diodes. *Appl. Phys. Lett.* **2014**, *105* (11), 113303.
26. Aonuma, M.; Oyamada, T.; Sasabe, H.; Miki, T.; Adachi, C. Material Design of Hole Transport Materials Capable of Thick-Film Formation in Organic Light Emitting Diodes. *Appl. Phys. Lett.* **2007**, *90* (18), 183503.
27. Owens, D. K.; Wendt, R. C. Estimation of the Surface Free Energy of Polymers. *J. Appl. Polym. Sci.* **1969**, *13* (8), 1741–1747.
28. Fusella, M. A.; Schreiber, F.; Abbasi, K.; Kim, J. J.; Briseno, A. L.; Rand, B. P. Homoepitaxy of Crystalline Rubrene Thin Films. *Nano Lett.* **2017**, *17* (5), 3040–3046.
29. Jurchescu, O. D.; Meetsma, A.; Palstra, T. T. M. Low-Temperature Structure of Rubrene Single Crystals Grown by Vapor Transport. *Acta Cryst.* **2006**, *B62* (2), 330–334.

Table 1: Glass Transition Temperatures and Surface Energies of Underlayers

Molecule	Bulk T_g [˚C]	Measured T_g for 70 nm Film [˚C]	Surface Energy [erg cm^{-2}]
Alq_3	178 [Ref. 22]	N/A	36.3 ± 2.2
NPB	95 [Ref. 23]	115	29.2 ± 3.4
TPTPA	83 [Ref. 24]	98[*)]	27.1 ± 0.4
m-MTDATA	75 [Ref. 23]	92	30.5 ± 3.9
MeO-TPD	67 [Ref. 25]	80	30.2 ± 5.3
TPD	58 [Ref. 26]	74	40.0 ± 5.6

[*)]Film for TPTPA T_g measurement is 80 nm.

Figures

(a)

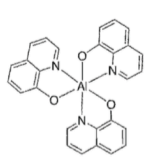

Alq_3

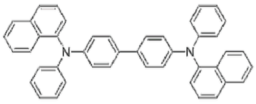

NPB

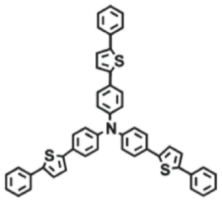

TPTPA

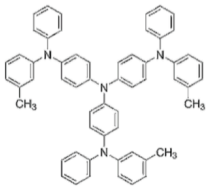

m-MTDATA

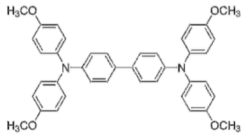

MeO-TPD

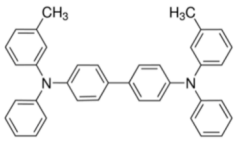

TPD

(b)

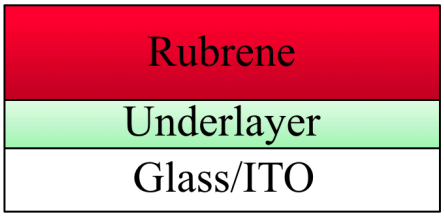

Figure 1. a) Molecular structures of the investigated underlayers; b) schematic of the sample stack showing rubrene deposited atop an underlayer.

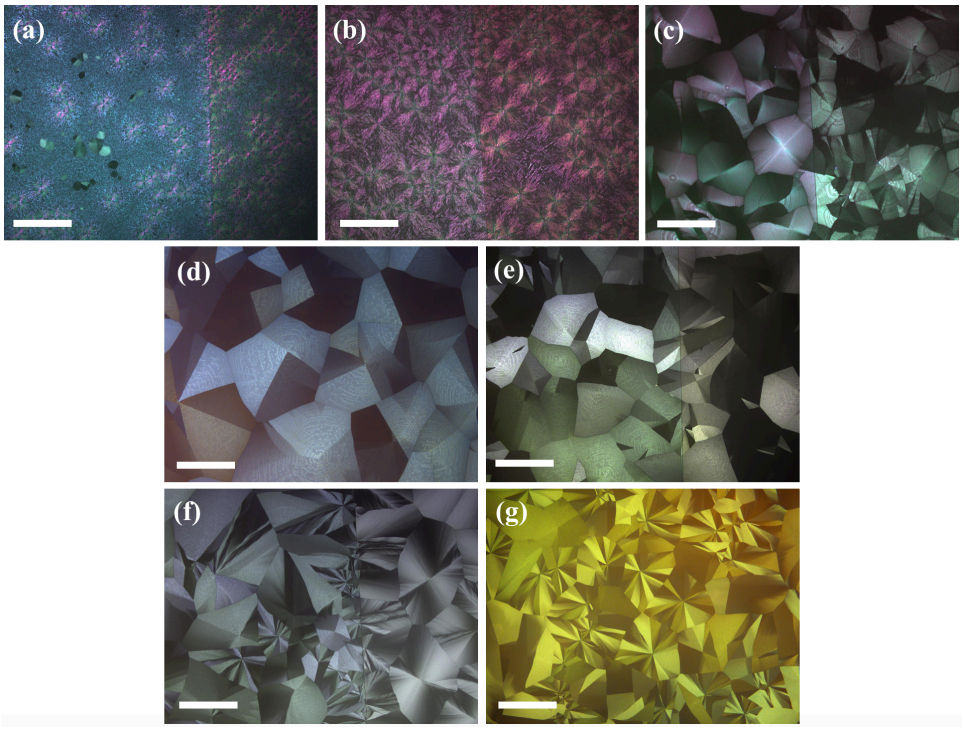

Figure 2. Series of polarized optical microscope images showing 20 nm rubrene films annealed at 140 ˚C with either a) no underlayer, or a 5 nm underlayer of b) Alq_3, c) NPB, d) TPTPA, e) m-MTDATA, f) MeO-TPD, or g) TPD. The high glass transition temperature (T_g) underlayers result in either the triclinic rubrene phase seen in b) and most of a), or orthorhombic spherulites seen in c). TPTPA and m-MTDATA possess optimal T_g and result in platelets, whereas MeO-TPD and TPD each have a low T_g that results in ray splitting. Scale bars are all 500 μm.

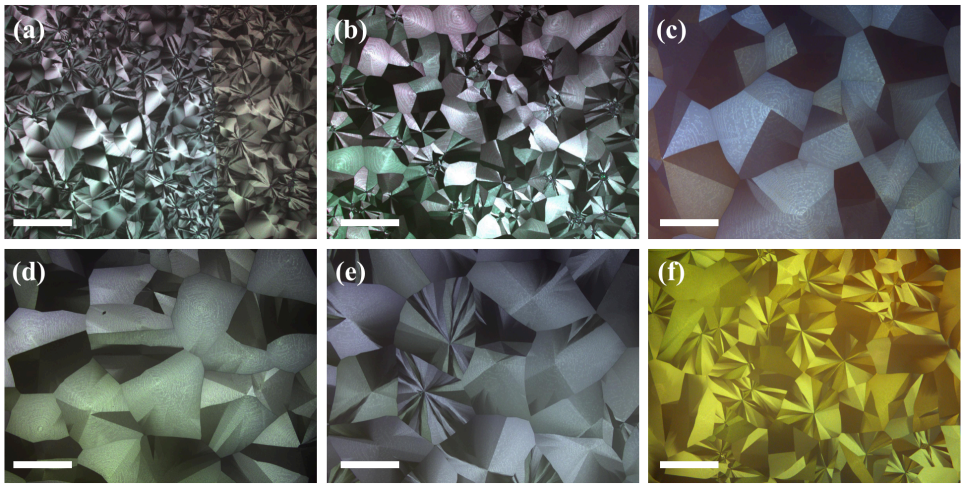

Figure 3. Series of polarized optical microscope images showing crystalline rubrene films with different underlayers (all 5 nm thick) grown under optimal conditions. The underlayer, rubrene thickness, and annealing temperatures are a) Alq_3, 40 nm, 160 ˚C; b) NPB, 30 nm, 150 ˚C; c) TPTPA, 20 nm, 140 ˚C; d) m-MTDATA, 20 nm, 140 ˚C; e) MeO-TPD, 20 nm, 140 ˚C; f) TPD, 20 nm, 140 ˚C. Scale bars are all 500 µm.

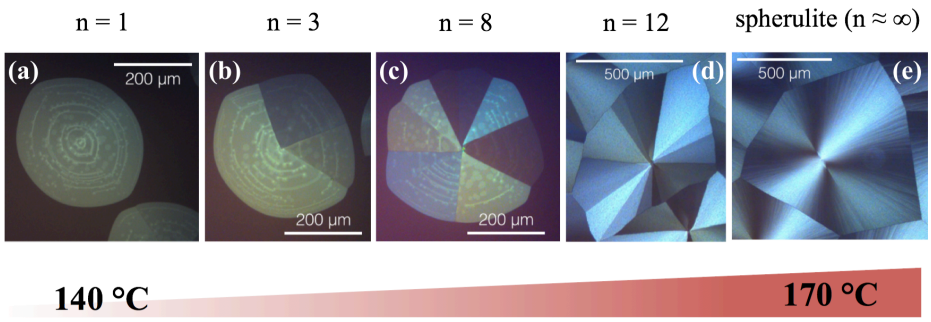

Figure 4. a-e) Sequence of polarized optical microscope images showing the trend that the average number of single-colored rays in a domain, *n*, increases with increasing annealing temperature until a spherulite is formed. The domains in a-c) are shown at the early stages of growth and are thus smaller than they would be in the complete films seen in d,e).

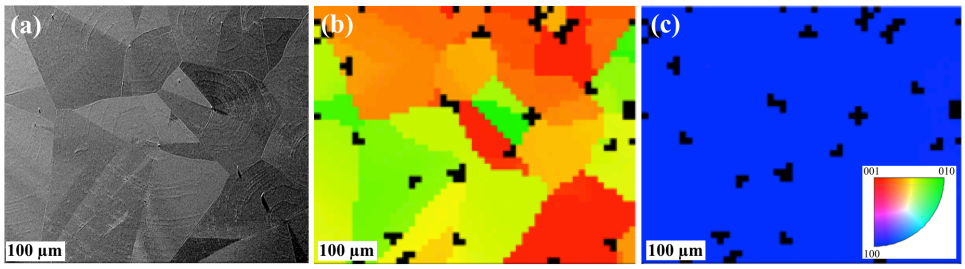

Figure 5. a) Scanning electron microscope image of a complete rubrene crystal film grown on a 5 nm TPTPA underlayer annealed at 140 ˚C displaying platelet crystallites that was used to collect data for the electron backscatter diffraction orientation; b) this orientation map identifies single crystal domains and shows how each domain is rotated in-plane with respect to each other; c) orientation map showing that the platelets are all oriented out-of-plane. The legend in (c) also applies to the map in (b).

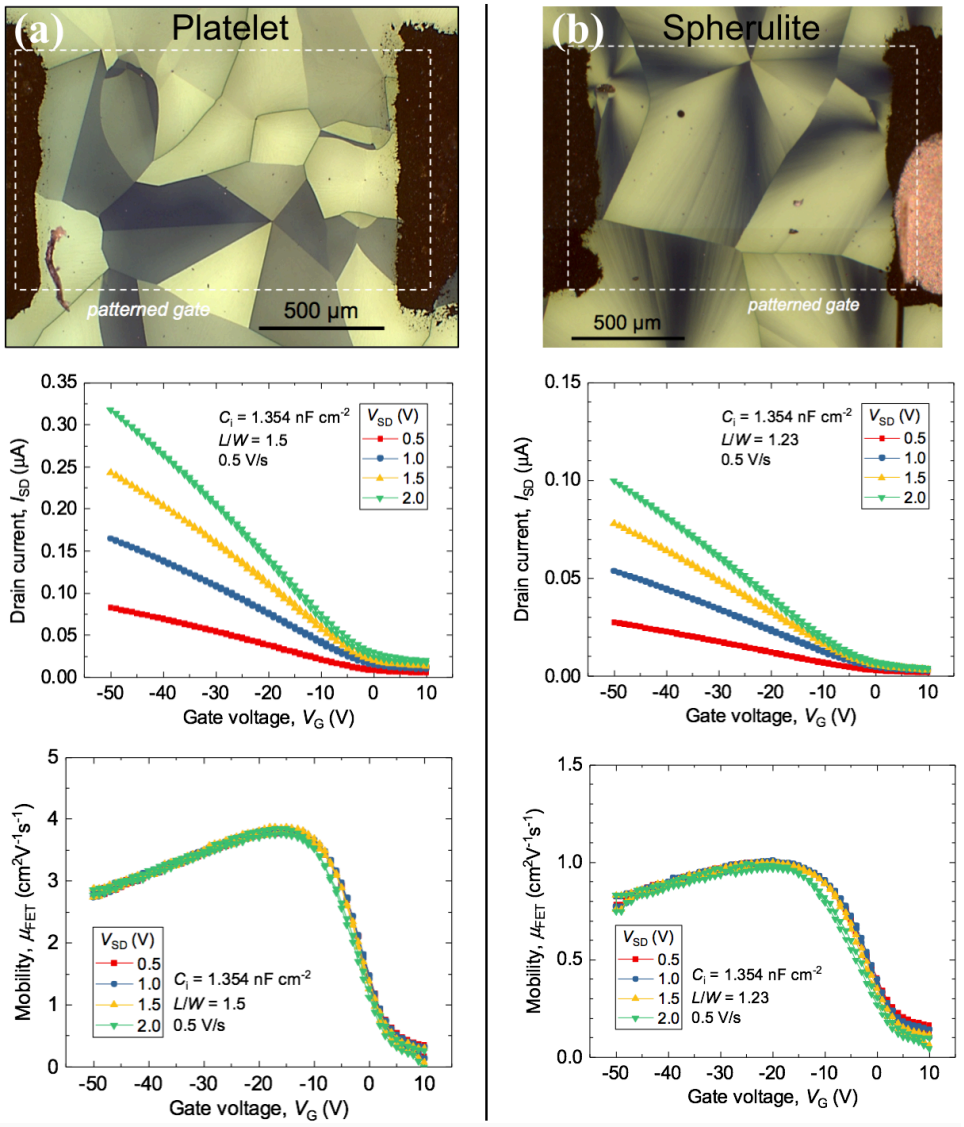

Figure 6. Polarized optical microscope images of the rubrene films around the conducting channel and plots of the source/drain current (I_{SD}) and FET mobilities in the linear regime (μ_{FET}) as a function of gate voltage (V_G) for two different morphologies of the rubrene layer: a) platelets, left column, and b) spherulites, right column.